Available online at www.sciencedirect.com
ScienceDirect
Lithos 91 (2006) 301–318
LITHOS
www.elsevier.com/locate/lithos

On the origin of microrhythmic layering in arfvedsonite lujavrite from the Ilímaussaq alkaline complex, South Greenland☆

John C. Bailey [a,*], Henning Sørensen [a], Tom Andersen [b], Lia N. Kogarko [c], John Rose-Hansen [a]

[a] *Geology Institute, University of Copenhagen, Øster Voldgade 10, DK-1350 Copenhagen K, Denmark*
[b] *Institutt for Geofag, Oslo University, P.O. Box 1047, Blindern, N-0316 Oslo, Norway*
[c] *Vernadsky Institute of Geochemistry and Analytical Chemistry, Russian Academy of Sciences, 19 Kosygin Street, Moscow 117975, Russia*

Received 11 July 2005; accepted 13 March 2006
Available online 5 June 2006

Abstract

Microrhythmic layering is locally developed in agpaitic arfvedsonite lujavrite from the Ilímaussaq alkaline complex, South Greenland. Three–15-cm-thick laminated dark layers alternate with 1–10-cm-thick, light-coloured granular urtitic layers. Dark layers are uniform (isomodal) but the urtitic layers are enriched in early nepheline and eudialyte in their lower parts and in late analcime and REE phosphate minerals in the upper parts. The layers are separated by sharp contacts; they are draped around rafts from the overlying roof zone and lack structures indicative of current processes or post-cumulus deformation. Compared with the background arfvedsonite lujavrite of the complex, the dark layers are richer in sodalite, microcline and arfvedsonite and poorer in analcime and eudialyte. They have higher K_2O, Cl, FeO* and S but lower Na_2O, H_2O^+, Zr and P contents, the opposite of the light-coloured layers. The complementary chemistry of the two types of layers oscillates about the composition of the background arfvedsonite lujavrite. Layers probably formed in a stagnant bottom layer of the lujavrite magma chamber. Each layer started as a liquid layer which exchanged components with the underlying crystallization front. On cooling, it crystallized primocrysts and exchanged components with the overlying magma which became a new, complementary liquid layer and, during further cooling and burial within the sequence of layers, it underwent largely closed-system interstitial crystallization. Exhaustion of Cl and a sharp decrease in a_{NaCl} relative to a_{H_2O} terminated the crystallization of a sodalite-rich dark layer and initiated abundant crystallization of nepheline in the overlying liquid layer (urtitic layer). The layered sequence represents a local K_2O-, Cl-rich but Na_2O-, H_2O-poor facies of arfvedsonite lujavrite and may have formed by exchanging components with sodalite-bearing rafts from the roof zone.

Keywords: Agpaitic; Lujavrite; Microrhythmic layering; Oscillatory crystallization; Volatile activities

1. Introduction

The intrusive complexes of the mid-Proterozoic Gardar igneous province, South Greenland, provide many examples of layered igneous rocks (Upton et al., 1996). In one of these complexes, the Ilímaussaq

☆ Contribution to the Mineralogy of Ilímaussaq no. 116.

* Corresponding author. Tel.: +45 35322411; fax: +45 35322440.
E-mail addresses: johnb@geol.ku.dk (J.C. Bailey), hennings@geol.ku.dk (H. Sørensen), tom.andersen@geo.uio.no (T. Andersen), kogarko@geokhi.ru (L.N. Kogarko), johnrh@geol.ku.dk (J. Rose-Hansen).

0024-4937/$ - see front matter © 2006 Elsevier B.V. All rights reserved.
doi:10.1016/j.lithos.2006.03.022

alkaline complex, the type locality of agpaitic rocks (Ussing, 1912), macro- and microrhythmic layering are displayed in an instructive way. Macrorhythmic layering exhibits layer thicknesses of metre scale; microrhythmic layering exhibits layer thicknesses of centimetre scale (Irvine, 1987).

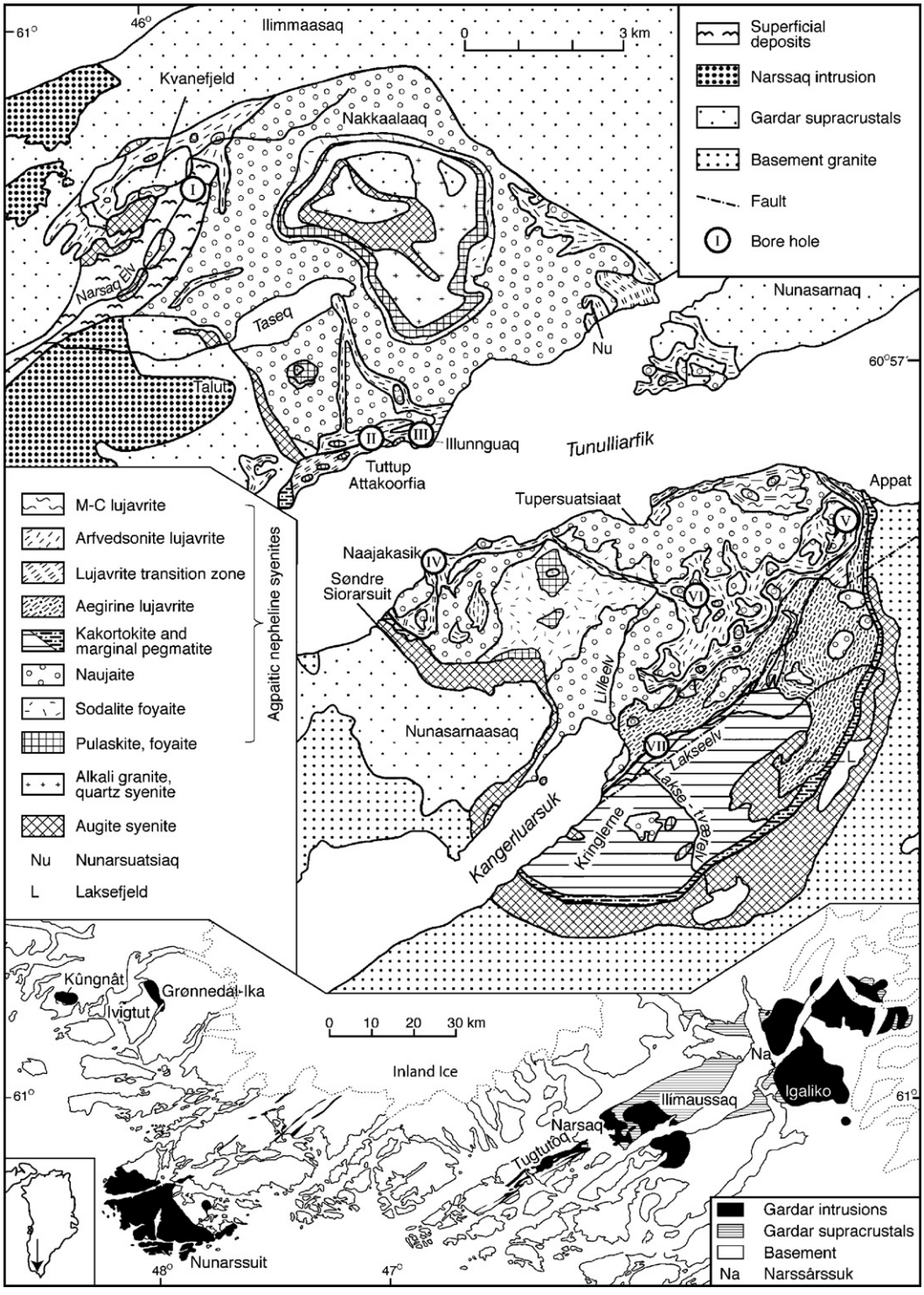

Fig. 1. Geological map of the Ilímaussaq alkaline complex with location of boreholes I to VII, from Sørensen (2001).

The most highly evolved rocks of the Ilímaussaq complex are lujavrites—meso- to melanocratic agpaitic nepheline syenites rich in eudialyte. Locally they display various types of layering which until now have been the subject of few studies (Sørensen, 1962; Ferguson, 1964; Bohse and Andersen, 1981; Bailey, 1995; Rose-Hansen and Sørensen, 2002). In the present paper, we focus on microrhythmic layering in arfvedsonite lujavrite. It consists of an alternation of laminated dark layers and granular light-coloured layers. The dark layers have the same modal composition and grain size throughout; they are uniform or isomodal according to Irvine (1987). The modal composition of the light-coloured urtitic layers varies from nepheline-rich to analcime-rich. Our petrogenetic assessment of these layers is set against a background of recent models for microrhythmic layering (e.g., Naslund and McBirney, 1996).

The Ilímaussaq complex was formed during three intrusive stages (Larsen and Sørensen, 1987). The agpaitic rocks belong to the third stage which consists of a roof series, and a floor series which evolved upwards into the intervening lujavrite series. The roof series crystallized downwards forming the succession pulaskite, foyaite, sodalite foyaite and naujaite. Naujaite is an agpaitic sodalite syenite (sodalitolite) which contains up to 75 vol.% cumulus sodalite. The exposed floor series is made up of kakortokite floor cumulates which show a macrorhythmic repetition of black, red and white layers. The lujavrite series is at least 500 m thick; its lowermost part is dominated by green varieties rich in aegirine, the upper part by black varieties rich in arfvedsonite (Ussing, 1912; Ferguson, 1964; Andersen et al., 1981; Bohse and Andersen, 1981; Rose-Hansen and Sørensen, 2002).

2. Layering in arfvedsonite lujavrite

The microrhythmic layering described here was briefly noted by Sørensen (1962) and Ferguson (1964). Similar layering has been observed at Appat (Bohse and Andersen, 1981: 60) and in drill core V (Fig. 1) (Rose-Hansen and Sørensen, 2002).

Our examination of layering has focused on well-exposed rocks at Tuttup Attakoorfia, on the north coast of Tunulliarfik (Fig. 1). This area belongs to the so-called breccia zone between the roof of naujaite and the underlying lujavrites (Ussing, 1912) in which rafts of naujaite from 1 m to several metres thick and up to scores of metres across are enclosed in and intruded by arfvedsonite lujavrite (Figs. 2–4).

At the westernmost part of Tuttup Attakoorfia, a succession of about 30 layered units can be seen in the 15–20-m-high coastal cliff (Figs. 3 and 4; Ferguson, 1964, Figs. 32, 35, 36). Dark layers, 3–15 cm or more thick, alternate with light-coloured layers, 1–10 cm thick.

The lujavrite layers drape over the enclosed naujaite rafts and are conformable with their upper and lower surfaces which have a near-horizontal orientation. Horizontal layers swing up and become parallel to the vertical ends of the rafts and curve over corners (Figs. 3 and 4). At one place, horizontal lujavrite layers approach the vertical side of a naujaite raft but the horizontal layers fade out 20–30 cm from the naujaite. The vertical contact against the naujaite is marked by thin layers parallel to the contact (Fig. 3). Lujavrite between naujaite rafts has been found as a fold structure; it appears as if partly consolidated lujavrite has been dragged down or down-folded where rafts have been fractured and drawn apart. Perfect vertical layering is developed parallel to the walls of the fracture (Fig. 4). This structure may also have been formed if lujavrite magma intruded the fracture from below and spread out over the two adjoining naujaite rafts.

Exposures do not permit an estimate of the thickness of the layered lujavrite series or an assessment of its relations with the overlying and underlying rocks. The absence of similar layering at appropriate depths in bore holes II and III, 500 m, respectively, west and east of Tuttup Attakoorfia (Fig. 1), indicates a limited lateral extension of the layered sequence.

3. Petrography

The microrhythmic layers were examined in many thin sections of samples collected in the horizontally layered lujavrites at the west end of Tuttup Attakoorfia (Fig. 4).

Contacts between dark and light-coloured layers are nearly always sharp (Figs. 5 and 6). However, there are irregularities in the form of fragments of dark layers enclosed in the lowermost part of the light-coloured layers (Fig. 5) and the upper contacts of the light-coloured layers are occasionally rather diffuse (Figs. 5 and 6). The dark layers are isomodal and generally more compact. The light-coloured layers display a range in modal composition but graded layering has not been observed. The density layering presented by Ferguson (1964, Fig. 36) is interpreted by us as arfvedsonite-rich sublayers.

Nepheline contents in the dark layers vary from 10 to 30 vol.%; their colour index is 40–60. Some of the light-coloured layers have >50 vol.% nepheline and a colour index of 15–40; they are urtite–ijolites. Examination in

Fig. 2. North coast of Tunulliarfik (Fig. 1) made up of lujavrites (black) with enclosed horizons of naujaite rafts (white) and overlain by naujaite. Tuttup Attakoorfia is the small dark coastal cliff to the left of the centre of photo.

UV light shows that the dark layers have up to 20 vol.% evenly distributed sodalite and the light-coloured layers <1 vol.%. The dark layers average about 35% arfvedsonite, 20% nepheline, 25% microcline, 10% sodalite, 5% analcime and 5% eudialyte. Albite is not present in these layers. The average composition of the light-coloured layers is about 25% nepheline, 15% arfvedsonite, 10% brown aegirine, 1% microcline, 35% analcime and 14% eudialyte, but this estimate is approximate because of the range in modal composition and content of late-magmatic analcime replacing felsic minerals.

Igneous lamination in dark layers is expressed by the parallel orientation of microcline tablets, prismatic arfvedsonite and platy eudialyte and is conformable to layer boundaries. The early crystals of nepheline, sodalite and the rarer microcline are slightly larger (0.4 to >1 mm) than the matrix minerals and are wrapped around by microcline tablets, about 0.2 mm long, and by platy eudialyte crystals, 0.4–0.6 mm across. Aggregates of acicular arfvedsonite are interstitial to nepheline, sodalite, eudialyte and microcline. There are no signs of post-cumulus deformation. Nepheline and sodalite contain inclusions of arfvedsonite and rare microcline.

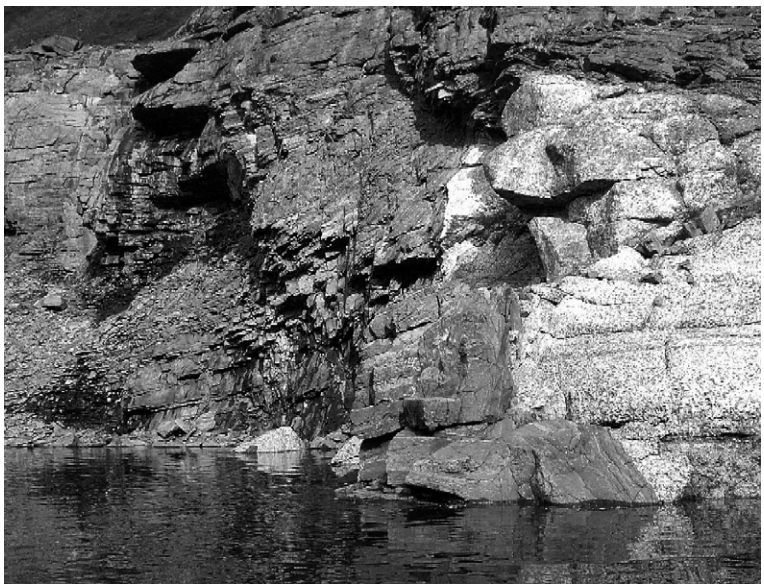

Fig. 3. Naujaite xenolith, about 8 m high, under fragmentation in layered lujavrite. The lujavrite layers drape the xenolith and rise steeply at its left side. Tuttup Attakoorfia. At the coast, a near-vertical contact between lujavrite and naujaite. Lujavrite layers are conformable with the contact, but away from the contact, layering disappears in a roughly 50-cm-wide zone and then reappears, but now as horizontal layers.

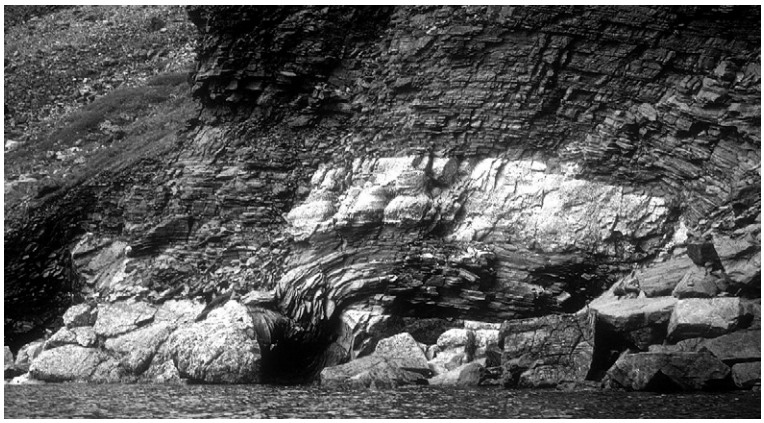

Fig. 4. Naujaite xenoliths (white) conformably wrapped by layered lujavrite which forms a fold structure between two xenoliths. Tuttup Attakoorfia, about 100 m west of Fig. 3. The naujaite raft above the fold is about 2 m thick. Note the regular alternation of thicker dark and thinner light-coloured layers in the lujavrite. The samples analysed were collected in the lujavrites to the left of the large naujaite raft.

Eudialyte occurs as euhedral crystals that lack inclusions and are partially overgrown by arfvedsonite. The nepheline and sodalite crystals are partly to completely replaced by analcime and/or natrolite. Central parts of large microcline crystals are often replaced by aggregates of fibrous natrolite. Otherwise, there is very little

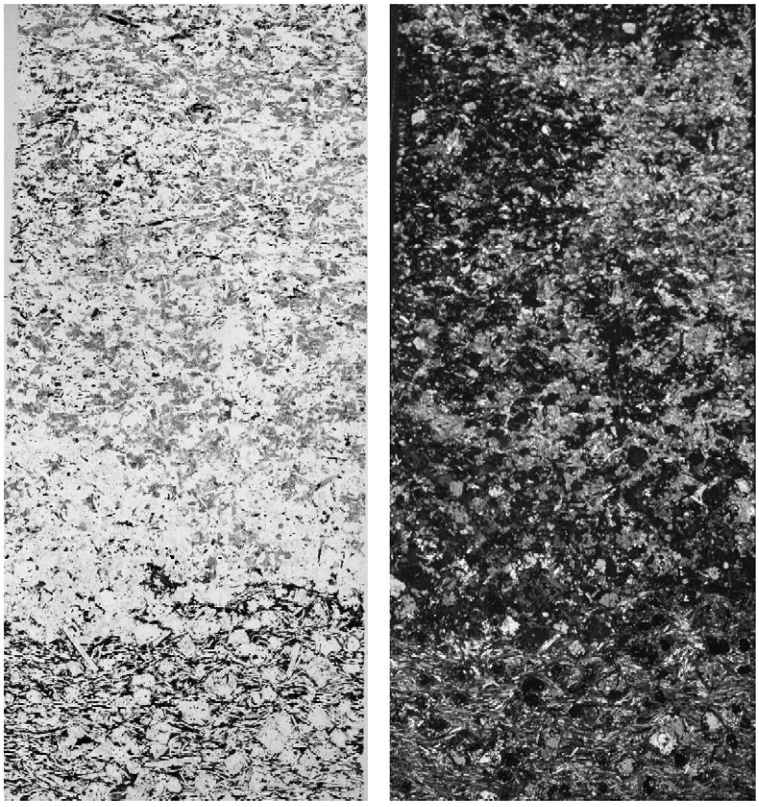

Fig. 5. Microphoto of the whole thin section. Sharp contact between dark layer and overlying light-coloured layer. Fragments of the dark layer are enclosed in the lower part of the light-coloured layer. Rounded analcime areas throughout the light-coloured layer mark the former presence of nepheline. In the uppermost part of the layer, these areas are mixed with areas showing the texture of the overlying dark layer. Sample 104384B, Tuttup Attakoorfia coast (1.7 × 4.2 cm, (a) plane polarized light, (b) crossed polars, analcime is black).

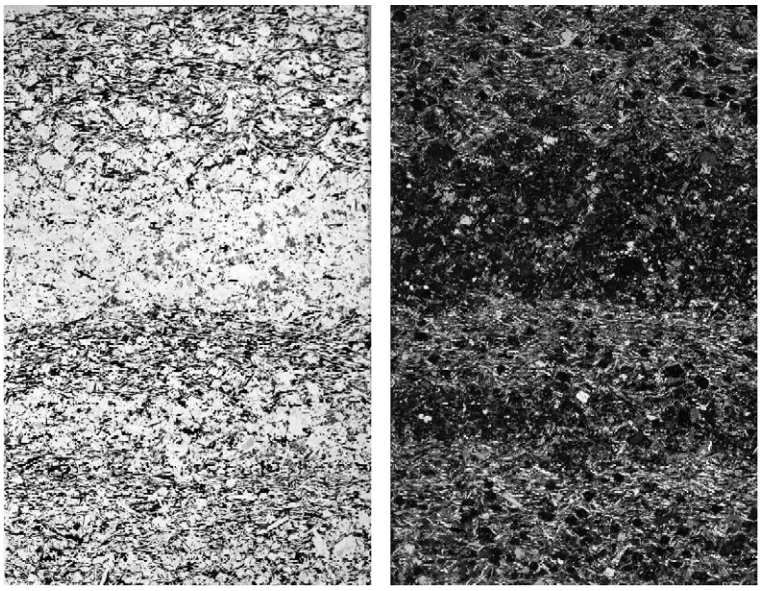

Fig. 6. Microphoto of the whole thin section. A granular, light-coloured layer of nepheline (mainly altered to analcime) and eudialyte (too small crystals to be seen) with minor arfvedsonite and microcline lying between two dark layers. The lower contact is sharp; the upper contact is more diffuse. There is a nepheline-/analcime-rich sub-layer in the lower dark layer. Sample 21067, Tuttup Attakoorfia coast (2.5 × 3.1 cm, (a) plane polarized light, (b) crossed polars, analcime is black).

analcime in the dark layers. Accessories are sphalerite, britholite ($(Ce,Ca,Sr)_2(Ce,Ca)_3(SiO_4,PO_4)_3(O,OH,F)$), and aggregates of monazite/rhabdophane that are interpreted as pseudomorphs after a vitusite-type mineral ($Na_3(Ce,La,Nd)(PO_4)_2$).

Nepheline and analcime secondary after nepheline form clusters and sub-layers in the dark layers (Fig. 6). The nepheline-rich sub-layers are also richer in eudialyte than the adjacent dark rock.

Some light-coloured layers are dominated by a framework of closely packed nepheline crystals under alteration to analcime (Figs. 5 and 6). The nepheline crystals are similar to those of the dark layers but have fewer arfvedsonite inclusions. Other light-coloured layers have a concentration of corroded nepheline crystals in their lower part and scattered smaller corroded nepheline grains enclosed in, and apparently pseudomorphed by, analcime in their upper part.

Overall, the light-coloured layers are poorer in sodalite, microcline and arfvedsonite, but richer in eudialyte, brown aegirine and REE phosphate minerals. Arfvedsonite occurs as scattered small stout crystals. Eudialyte crystals are texturally similar to those in the dark layers, and are concentrated up to 25 vol.% in the lowermost parts of the layers. The top parts of the layers are richer in the REE phosphate minerals britholite and monazite/rhabdophane. Brown aegirine often occurs throughout the layers (Fig. 5) in the form of a patchy network and is at least partly formed at the expense of arfvedsonite. It is accompanied by late microcline, analcime and very scarce albite laths.

In the uppermost part of some light-coloured layers there are patches with textures similar to that of the dark layers (Fig. 6). The microcline of the patches is partly replaced by new, late microcline and by analcime; the arfvedsonite is partly replaced by brown aegirine. These minerals also occur in the lower part of the overlying dark layer.

The modal composition of the light-coloured layers varies considerably. Some layers (e.g., 104384C) are less distinctly segregated from the dark layers. They are poorer in nepheline and eudialyte and have retained a microcline–arfvedsonite framework similar to that of the dark layers. They contain small amounts of sodalite.

4. Whole-rock chemistry

Major-element analyses were obtained by XRF techniques, and FeO by the vanadate method (Kystol and Larsen, 1999). Contents of trace elements including Cl and S were analysed directly on pressed powder pellets by XRF using a Philips PW1400 spectrometer and the techniques of Norrish and Chappel (1977). In addition, REE, Cs, Hf, Ta and Co were analysed by INAA and ICP-MS, Li and Be by

atomic absorption, F by a specific-ion electrode, and H_2O by CHN chromatography.

Five dark and four light-coloured layers were cut out and analysed for major and trace elements (Table 1, GI. 104384A, B, C). Samples A1, A3, A5 are three successive dark layers, samples A2 and A4 the interspaced light-coloured layers. Layers B and C are from separate samples.

The dark layers are relatively homogeneous, whereas the light-coloured layers are chemically more variable (Fig. 7). Relative to the light-coloured layers, the dark layers are richer in FeO*, MnO, Ge and Li due to higher contents of arfvedsonite, richer in K_2O, Rb and Tl due to higher microcline contents, and richer in Cl, S and Br due to higher sodalite contents. They have lower levels of Fe_2O_3/FeO due to lower contents of brown aegirine relative to arfvedsonite, lower Na_2O due to lower levels of nepheline and analcime, and lower H_2O^+, Cs and Be due to lower levels of analcime and natrolite.

The light-coloured layers are characterized by remarkably high contents of ZrO_2 and P_2O_5 (Fig. 7). The bulk of Zr, Hf, Ca, Ba, Sr, Eu, HREE, Y, Nb, Ta, Th, U and Cl is contained in eudialyte and the bulk of P and LREE is contained in the REE phosphates monazite/rhabdophane and britholite. The light-coloured layers–especially the bottom part–have lower La/Yb_N ratios than the dark layers (24–37 vs. 26–88) (Fig. 8). This reflects the higher ratio of eudialyte over REE phosphates in the light-coloured layers. In Ilímaussaq, eudialyte is relatively less enriched in LREE than REE phosphates (Semenov, 1969).

The range of H_2O^+ contents in dark layers (0.90–1.66 wt.%) lies well below levels in arfvedsonite lujavrites (2.8–4.7 wt.%) reflecting the low contents of interstitial zeolites. H_2O^+ contents in light-coloured layers (2.77–4.39 wt.%) generally lie above the H_2O content in the freshest arfvedsonite lujavrite (3.05 wt.%) (Table 2) but cover the same range as in typical arfvedsonite lujavrites which include zeolitized samples. H_2O^+ correlates positively with Zr ($r=0.93$) and P (0.86) but negatively with Cl (−0.90) and S (−0.77) (Table 1). The wettest light-coloured layers are richest in Zr and P whereas the driest dark layers are richest in Cl and S.

One of the analysed light-coloured layers, 104384C, shows a less pronounced concentration of nepheline and eudialyte and has a higher microcline content than the three other analysed light-coloured layers. This is confirmed chemically by its higher contents of K_2O and lower contents of CaO and ZrO_2 (Table 1).

In light-coloured layers, the lower part is rich in nepheline and eudialyte and has high Na + K, Al, Ca, Zr, Rb, Ba, Y and Nb. It also has fairly low FeO* and Fe_2O_3/FeO ratios (0.77) because arfvedsonite is only slightly altered to aegirine. The upper part shows lower contents of the components of nepheline and eudialyte and higher contents of the components of REE phosphate minerals. This is reflected in the higher La/Yb_N ratios in the upper part of the layers (Fig. 8). The arfvedsonite is strongly altered to aegirine which explains the high Fe_2O_3/FeO ratio (0.98).

The almost constant element ratios Zr/U (27–44), Zr/Y (6.4–7.0) and K/Rb (27–39) for the dark and light-coloured layers suggest that the minerals controlling these ratios (eudialyte, microcline) are not changing their chemistry but are simply changing their mutual proportions in the different layers. In detail, subtle increases in Zr/Hf and Nb/Ta ratios within the light-coloured layers are consistent with the fractionation of low-Zr/Hf-Nb/Ta eudialyte.

The bulk composition of the layered lujavrites was estimated by combining the chemical compositions of dark and light-coloured layers in a 3:1 ratio (Table 2, Fig. 7). This ratio allows for the greater thickness of the dark layers. The recombined analysis reproduces most features of average (background) arfvedsonite lujavrite of this part of the complex (Table 2) but differs in markedly higher contents of K_2O, Rb, Tl, FeO*, Cl, Br, S, Ba, Pb, Mo and Zn and lower contents of Al_2O_3, Na_2O, ZrO_2, P_2O_5 and H_2O^+. The Na/K ratio for average arfvedsonite lujavrite (2.99) is intermediate between the average values for dark (1.24) and light-coloured layers (4.19), but distinctly higher than that of the recombined analysis (1.59). The ZrO_2 content of the dark layers (0.31%) is lower and the content of the light-coloured layers (1.39%) is higher than the average level in arfvedsonite lujavrite (0.83%). The same contrast is shown by the P_2O_5 contents. Perhaps the largest difference between the recombined analysis and the average analysis is the higher Cl and S contents of the former. In general, the dark and light-coloured layers display a complementary chemistry with their contents of virtually all major and trace elements lying on either side of the average analysis.

5. Phase relations

Agpaitic Ilímaussaq melts consolidated at about 1 kbar P_{H_2O} (Konnerup-Madsen and Rose-Hansen, 1984; Markl et al., 2001). The lujavrite liquidus and solidus temperatures at 1 kbar P_{H_2O} have been estimated, respectively, as 885 °C and 430 °C (Piotrowski and Edgar, 1970) or as 750 °C and 450–500 °C (Markl et al., 2001), which is an interval of

Table 1
Chemical analyses of layered arfvedsonite lujavrites, Tuttup Attakoorfia (D=dark layer, L=light-coloured layer)

	104384														
	A1	A2	A2-1	A2-2	A3	A4	A4-1	A4-2	A5	B1	B2	B2-1	B2-2	C1	C2
	D	L	L	L	D	L	L	L	D	D	L	L	L	D	L
SiO_2	51.35	50.11	49.81	50.18	51.63	49.62	50.07	50.97	51.56	51.18	51.66	50.14	51.95	52.87	50.57
TiO_2	0.31	0.23	0.26	0.24	0.28	0.27	0.32	0.30	0.30	0.27	0.25	0.28	0.22	0.31	0.28
ZrO_2	0.32	1.85	2.07	1.55	0.34	2.23	2.23	1.80	0.48	0.28	1.89	2.84	1.59	0.11	1.00
Al_2O_3	13.06	13.85	14.67	13.05	12.72	12.51	12.56	11.92	13.22	13.69	12.31	13.70	11.85	12.04	13.35
Fe_2O_3	3.73	4.15	3.74	4.24	4.47	5.19	5.35	5.63	4.80	4.05	5.91	3.62	6.41	4.86	4.49
FeO	10.78	5.24	4.57	6.27	10.09	5.21	4.12	4.15	9.71	10.36	3.73	3.47	4.47	11.10	8.34
MnO	0.52	0.51	0.51	0.49	0.53	0.53	0.55	0.53	0.54	0.53	0.52	0.60	0.52	0.55	0.52
MgO	0.09	0.02	0.07	0.07	0.10	0.05	0.05	0.10	0.08	0.07	0.12	0.18	0.10	0.09	0.07
CaO	0.35	1.17	1.24	0.99	0.35	1.13	1.24	1.09	0.42	0.32	1.18	1.63	1.03	0.21	0.74
Na_2O	8.33	11.69	11.65	11.48	7.97	11.13	11.36	9.94	8.78	8.91	10.36	12.16	9.99	7.19	10.95
K_2O	5.79	1.85	2.20	1.47	5.94	1.65	1.69	2.98	5.26	5.71	3.20	1.83	3.21	6.91	2.71
P_2O_5	0.18	0.47	0.42	0.63	0.23	0.80	0.70	0.87	0.17	0.17	0.54	0.40	0.64	0.17	0.34
H_2O^+	1.46	4.04	4.11	4.27	1.44	4.10	4.06	3.03	1.66	1.50	2.82	4.39	2.77	0.90	3.27
H_2O^-	0.46	0.44	0.65	0.53	0.41	0.52	0.50	0.50	0.45	0.32	0.55	0.57	0.45	0.41	0.46
S	0.24	0.15	0.12	0.19	0.26	0.18	0.18	0.23	0.19	0.22	0.24	0.10	0.24	0.27	0.21
Cl	0.44	0.08	0.09	0.04	0.34	0.05	0.05	0.04	0.26	0.41	0.05	0.08	0.04	0.40	0.16
F	0.15	0.15	0.14	0.14	0.12	0.14	0.12	0.17	0.16	0.13	0.13	0.12	0.12	0.12	0.14
Others	1.56	3.21	3.18	3.71	1.72	4.25	4.19	4.55	1.66	1.43	3.76	3.45	3.98	1.50	2.52
	99.12	99.38	99.69	99.68	98.94	99.75	99.55	98.97	99.72	99.55	99.38	99.84	99.72	100.01	100.19
–O	0.28	0.16	0.14	0.16	0.26	0.15	0.15	0.20	0.22	0.26	0.19	0.12	0.18	0.28	0.20
	98.84	99.22	99.55	99.52	98.68	99.60	99.40	98.77	99.50	99.29	99.19	99.72	99.54	99.73	99.99
A.I.	1.53	1.53	1.47	1.57	1.54	1.61	1.63	1.64	1.52	1.52	1.67	1.60	1.68	1.60	1.57
Cs	6.2	57	51	63	8.8	51	51	36	13	8.2	31	51	35	2.9	48
Rb	1370	459	614	329	1410	421	510	875	1270	1320	848	557	853	1600	577
Tl	5.0	1.2	1.7	0.7	4.8	0.7	0.9	1.3	4.2	6.3	1.9	1.3	2.0	5.0	2.2
Ba	125	179	204	151	123	191	218	183	124	105	183	224	157	118	144
Pb	870	627	597	737	864	739	674	738	891	791	602	492	684	989	826
Sr	48	124	127	122	50	140	144	141	56	46	129	142	126	38	88
La	1270	4755	4345	5979	1652	6772	6421	6883	1332	1151	5353	4383	6050	1014	3280
Ce	1878	7649	7264	8851	2381	10,173	9815	10,757	2140	1740	8630	8236	9293	1288	5149
Pr	188	772	795	830	233	946	958	974	224	172	852	910	872	111	473
Nd	583	2760	2762	2777	703	3112	3314	3277	730	530	2975	3510	2871	309	1594

Sm	83.8	468	500	402	94.5	469	547	480	117	73.5	486	710	418	33.3	251
Eu	7.1	40.1	43.9	33.3	7.9	39.6	47.1	40.0	10.4	6.4	41.3	62.9	34.8	2.7	19.5
Gd	69.5	390	387	367	74.7	388	463	401	99.5	60.2	419	618	343	25.6	201
Tb	9.7	56.5	62.6	46.9	10.7	56.7	67.5	57.2	14.5	8.7	59.0	91.9	48.3	3.6	29.1
Dy	49.6	300	334	243	53.9	294	355	294	76.6	44.1	308	500	247	16.6	157
Ho	9.1	56.5	62.8	43.4	9.6	54.1	65.9	53.0	14.2	7.9	56.3	94.7	44.6	2.8	29.3
Er	25.0	150	167	117	26.0	143	176	144	38.3	21.5	151	249	121	8.1	77.8
Tm	3.6	21.9	24.5	16.7	3.8	20.7	25.5	20.4	5.7	3.1	21.5	36.5	16.8	1.2	11.3
Yb	22.6	134	148	101	23.5	125	155	123	34.9	19.4	130	218	101	7.8	67.6
Lu	3.0	16.7	18.9	12.8	3.1	15.8	19.6	15.5	4.6	2.5	16.3	27.2	12.7	1.1	8.7
Y	362	2050	2310	1640	380	1960	2430	1950	558	316	2080	3280	1690	124	1090
Th	38	232	272	174	49	228	294	232	68	36	245	452	182	24	101
U	73	348	391	262	72	328	400	312	112	79	357	587	276	21	196
Zr	2380	13,700	15,300	11,500	2510	13,300	16,500	13,300	3590	2100	14,000	21,000	11,800	813	7400
Hf	27.5	169	188	136	29.1	161	201	161	38.9	24.0	169	270	138	9.6	82.5
Sn	82	404	472	304	85	393	389	404	132	70	422	306	449	45	233
Nb	820	1530	1650	1150	732	1500	1620	1320	799	1020	1490	2000	1280	617	1080
Ta	25.1	107	120	79.8	24.1	103	123	98.6	30.7	28.1	106	173	84.3	11.1	57.0
Li	765	411	367	445	755	419	360	343	747	774	362	286	345	890	712
Zn	3330	3320	2810	5060	3630	5380	4640	5930	3620	2830	4130	2000	4990	4340	3880
Co	0.8	0.5	0.4	0.4	0.4	0.7	0.5	0.5	0.9	0.4	0.4	0.5	0.6	1.3	0.4
Ga	91	96	101	94	91	88	90	96	92	98	96	92	95	82	91
Ge	3.3	1.6	1.5	2.1	3.2	2.0	1.7	1.9	3.2	3.1	1.8	1.4	1.9	3.4	2.5
Be	34	123	110	136	41	128	116	91	60	41	88	113	79	23	108
Mo	96	21	17	22	95	12	12	13	63	65	9.7	8.0	10	14	17
As	31	19	17	18	31	17	17	17	31	16	11	10	12	19	15
F	1480	1480	1440	1440	1240	1400	1240	1680	1560	1320	1320	1240	1180	1240	1400
Cl	4380	810	850	440	3360	530	520	370	2580	4130	500	760	420	4020	1620
Br	1.4	0.5	0.5	0.3	1.0	0.2	0.2	0.3	0.6	1.1	0.2	0.3	0.2	1.1	0.3
S	2410	1490	1180	1860	2560	1770	1790	2260	1930	2200	2360	1000	2370	2650	2100
K/Rb	35	33	30	37	35	33	28	28	34	36	31	27	31	36	39
La/Yb_N	38.3	24.2	19.9	40.4	47.9	36.9	28.2	38.1	25.9	40.3	28.0	13.6	40.7	88.5	33.0
Zr/Hf	86.5	81.1	81.4	84.6	86.3	82.6	82.1	82.6	92.3	87.5	82.8	77.8	85.5	84.7	89.7
Nb/Ta	32.7	14.3	13.8	14.4	30.4	14.6	13.2	13.4	26.0	36.3	14.1	11.6	15.2	55.6	18.9
Zr/U	33	39	39	44	35	41	41	43	32	27	39	36	43	39	38
Zr/Y	6.6	6.7	6.6	7.0	6.6	6.8	6.8	6.8	6.4	6.6	6.7	6.4	7.0	6.6	6.8

A.I. $(Na_2O+K_2O)/Al_2O_3$ mol. Analysts: J.C. Bailey, Birgit Damgaard and Rock Geochemistry Laboratory of the Denmark and Greenland Geological Survey. Others: sum of other trace elements as oxides.

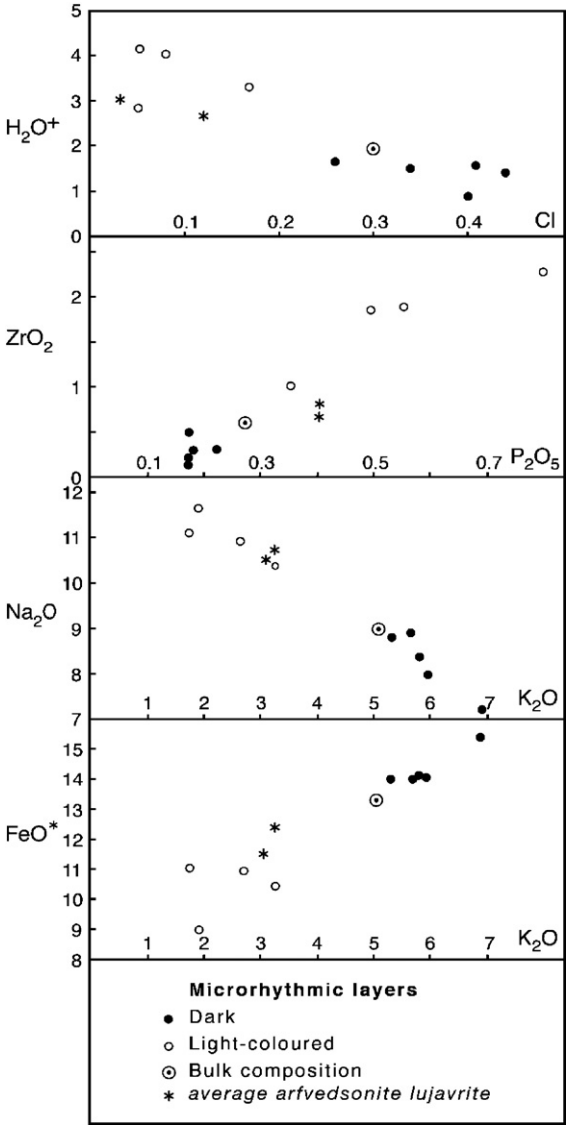

Fig. 7. Two-element plots of dark and light-coloured layers. Note that the two types of layers oscillate about the composition of the average arfvedsonite lujavrite (Gerasimovsky, 1969; our unpublished data). The bulk composition is dominated by the dark layers and deviates significantly from the average lujavrite.

consolidation of more than 250 °C. In the late stage of crystallization of lujavrite melts, analcime is stable at a water activity of 0.7–1.0 and a NaCl activity less than 0.1 (Markl et al., 2001).

Experimental results in residual systems such as Ab–Or–Q (Tuttle and Bowen, 1958), Na_2O–Al_2O_3–Fe_2O_3–SiO_2 (Bailey and Schairer, 1966; Gittins, 1979; Korobeinikov et al., 1998), and Ab–Ne–Ac–Di–H_2O (Nolan, 1966; Edgar and Nolan, 1966; Edgar, 1974) are relevant to the crystallization history of the layered lujavrites. However, none of these experimental systems have more than five components. The ideal compositions of the major rock-forming minerals of the layered lujavrite–microcline (Mic, $KAlSi_3O_8$), nepheline (Ne, $Na_3K(AlSiO_4)_4$), sodalite (Sod, $(Na_4(AlSiO_4)_3Cl$), analcime (Anl, $NaAlSi_2O_6{\cdot}H_2O$), arfvedsonite (Arf, $Na_3Fe_5Si_8O_{22}(OH)_2$) and aegirine (Aeg, $NaFeSi_2O_6$)–require (at least) eight chemical components (Si–Al–Fe–Na–K–O–H–Cl or SiO_2–Al_2O_3–FeO–Fe_2O_3–Na_2O–K_2O–H_2O–NaCl). The chemographic relations within the eight-component system may be illustrated in the volatile-free SiO_2–$AlO_{1.5}$–($KO_{0.5}$+$NaO_{0.5}$)–FeO_t tetrahedron (Fig. 9). All solid phases considered in this study plot on the outside faces or along the edges of the tetrahedron. In this projection, whole-rock compositions lie on a trend from Arf-rich dark layers to Ne+Eud-rich light-coloured layers. Note that, as long as arfvedsonite is the only iron-bearing mineral crystallizing, oxygen fugacity remains unconstrained by local mineral-melt equilibria.

Although the crystallization of the magma is ultimately driven by cooling, the mineralogy of the cumulate assemblages at any time is largely controlled

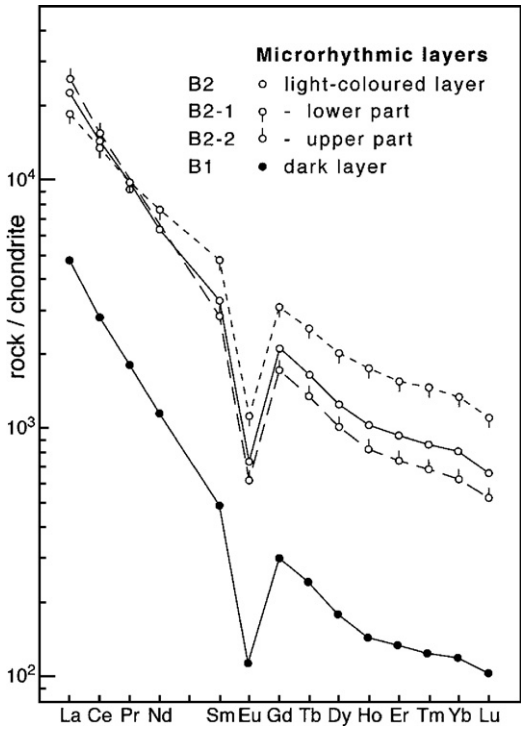

Fig. 8. Chondrite-normalized (McDonough and Sun, 1995) REE patterns of adjacent dark and light-coloured layers in sample 104384B. The upper part of the light-coloured layer (rich in REE phosphates) has a steeper pattern than the lower part (rich in eudialyte).

Table 2
Average composition of dark and light-coloured layers and a 3:1 recombination of analyses of dark and light-coloured layers, Tuttup Attakoorfia, and average analyses of arfvedsonite lujavrites from the Tunulliarfik area (7) and from Gerasimovsky (1969) (6) (wt.% and ppm)

	Dark layers (5)	Light-coloured layers (4)	Dark and light-coloured layers 3:1	Average composition arfvedsonite lujavrite (7)	Average composition arfvedsonite lujavrite (6)
SiO_2	51.72	50.49	51.41	52.01	52.89
TiO_2	0.29	0.26	0.28	0.17	0.35
ZrO_2	0.31	1.39	0.58	0.83	0.64
Al_2O_3	12.95	13.01	12.97	13.80	14.59
Fe_2O_3	4.38	4.94	4.52	4.85	6.30
FeO	10.41	5.63	9.21	7.17	6.77
MnO	0.53	0.52	0.53	0.53	0.41
MgO	0.09	0.22	0.12	0.12	0.54
CaO	0.33	1.06	0.51	0.42	0.39
Na_2O	8.24	11.03	8.94	10.59	10.72
K_2O	5.92	2.35	5.03	3.06	3.28
P_2O_5	0.18	0.54	0.27	0.41	0.41
H_2O^+	1.39	3.56	1.93	3.95 [a]	2.67
H_2O^-	0.41	0.49	0.43	0.21	n.a.
S	0.24	0.20	0.23	0.12	0.14
Cl	0.37	0.09	0.30	0.03	0.12
F	0.14	0.14	0.14	0.14	0.20
Others	1.59	3.44	2.05	1.34	n.d.
	99.47	99.36	99.44	99.63	100.31
–O	0.26	0.18	0.24	0.13	0.18
	99.21	99.18	99.20	99.50	100.13
FeO*	14.35	10.08	13.28	11.54	12.44
Agpaitic index	1.54	1.61	1.56	1.50	1.53
Rb	1394	576	1190	644	630
Ba	119	174	133	38	50
Pb	831	699	798	534	422
Sr	48	120	66	71	58
La	1470	5190	2400	3260	2280
Ce	2000	8290	3572	4770	3330
Nd	614	2780	1155	1630	900
Y	348	1800	711	912	480
Th	43	202	83	287	72
U	71	238	113	201	178
Zr	2280	11,400	4560	6144	3640
Nb	798	1280	918	628	339
Li	786	476	708	640	791
Zn	3550	4180	3707	1980	2074
Ga	90	93	91	127	104
Be	40	112	58	47	35

Numbers in brackets are number of analyses.
[a] 3.05% in two non-zeolitised samples.

by composition-dependent intensive parameters (Markl et al., 2001; Andersen and Sørensen, 2005). Lack of thermodynamic data for liquidus minerals and highly alkaline silicate liquids prohibits quantitative characterization of liquidus mineral equilibria in P–T–X space. It is, however, possible to evaluate the relative stability of liquidus phase assemblages in general isobaric–isothermal activity diagrams. Arfvedsonite is not involved in mineral reactions with the other liquidus minerals; Fe may therefore be disregarded, and the stability relationships of the cumulate assemblages may be analyzed in terms of the simplified felsic system SiO_2–K_2O–Al_2O_3–H_2O–NaCl. In this simplified system, oxygen fugacity only has an indirect control on the stability of liquidus mineral assemblages through its control on water activity. Four divariant, three univariant and one invariant phase assemblages at constant pressure and temperature can be defined in the silica-undersaturated part of the system (Table 3). Of these assemblages, only the albite-free assemblages ii, iii, iv and v are directly relevant to the crystallization of the layered lujavrites (Table 3a). The stability fields of the critical phase

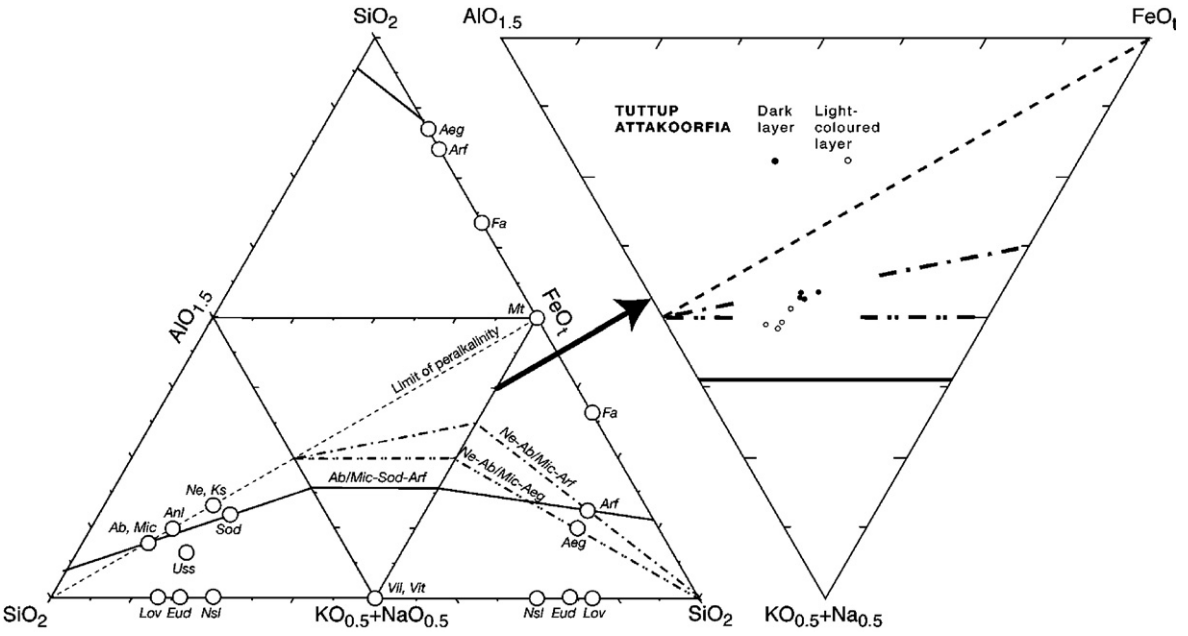

Fig. 9. Whole-rock and ideal mineral compositions in layered lujavrite projected to the volatile-free SiO_2–$AlO_{1.5}$–($KO_{0.5}$+$NaO_{0.5}$)–FeO_t tetrahedron, shown in an unfolded state. The minerals (larger circles) are Ab: albite; Aeg: aegirine; Anl: analcime; Arf: arfvedsonite; Eud: eudialyte; Fa: fayalite; Ks: kalsilite; Lov: lovozerite; Mt: magnetite; Mic: microcline; Ne: nepheline; Nsl: natrosilite; Sod: sodalite; Uss: ussingite; Vil: villiaumite; Vit: vitusite. The broken lines are the intersections of planes through the tetrahedron with the outer faces; Ne–Ab/Mic–Arf, Ne–Ab/Mic–Aeg and Ab/Mic–Sod–Arf are potential thermal divides in the system. The plane Ab/Mic–Anl–Ne/Ks marks the limit of peralkalinity.

assemblages in SiO_2–H_2O–NaCl activity space are shown in Fig. 10.

Since K is an essential component in natural nepheline, the classical three-phase Ne–Ab–silica buffer assemblage in the Si–Al–Na–O system (e.g., Carmichael et al., 1974) is replaced by a four-phase assemblage Ne+Ab+Mic+LL. This assemblage is only stable within part of the front face of the activity prism shown in Fig. 10a and b. In the interior part of the diagram, albite is not a stable member of the phase assemblages of the K-rich, Na-poor layered lujavrites.

Reactions B and C (Table 3c) and mineral assemblages iii, iv and v (Table 3b) with analcime are only stable at low temperatures ($T \leq 525$ °C; Fig. 10b; Markl et al., 2001). At elevated temperatures ($T > 525$ °C; Fig. 10a), analcime does not appear as a liquidus mineral, and only liquidus phase assemblages with Ne, Ab, Mic and Sod (+Arf and eudialyte) need to be considered. Assemblages i and ii (Table 3b) define two divariant planes, one (ii) within the volume shown in Fig. 10a, and one (i) coinciding with the low-a_{NaCl} part of the front face. At lower temperatures ($T \leq 525$ °C), analcime becomes stable on the liquidus at elevated water activity (Fig. 10b). The stability field of Anl+Mic is situated at higher water activity than the other liquidus assemblages considered here and is separated from the primary fields of anhydrous liquidus assemblages by divariant planes iii and iv (Table 3b; Fig. 10b).

6. Discussion

6.1. Layering processes

Three major groups of processes have been proposed to account for the formation of igneous layering (Naslund and McBirney, 1996): (1) dynamic processes in which crystals are added to the crystallization site or intercumulus melts are squeezed away (Ussing, 1912; Wager and Brown, 1968); (2) non-dynamic in situ, largely early magmatic processes such as varying rates of diffusion, nucleation, growth and so on (Wager, 1959; Maaløe, 1978; McBirney and Noyes, 1979); and (3) non-dynamic in situ processes largely of a late or post-magmatic character such as compaction or crystal aging (Boudreau, 1995; Boudreau and McBirney, 1997).

In the layering studied here, the sharp contacts between layers, the occurrence of vertical layers, the lack of graded layering or signs of deformation are hard to explain by crystal-liquid separation mechanisms. Instead, the discussion will mainly consider processes capable of forming in situ layering at an early magmatic stage.

Table 3
Liquidus phase assemblages in lujavritic liquid

(a) Observed liquidus phase assemblages in layered lujavrite		
Normal lujavrite paragenesis:		
	Ne+Arf+Ab+Mic	
Tuttup Attakoorfia layered lujavrite:		
	Light: Ne (+Arf+Mic)	
	Dark: Ne+Arf+Sod+Mic	
(b) Low-variance liquidus assemblages in the system SiO_2–K_2O–Al_2O_3–SiO_2–H_2O–NaCl		
i:	Ne+Ab+Mic+LL	($F_{T,P}$=2)*
ii:	Ne+Sod+Mic+LL	($F_{T,P}$=2)
iii:	Ne+Anl+Mic+LL	($F_{T,P}$=2)
iv:	Sod+Anl+LL	($F_{T,P}$=2)**
v:	Ne+Sod+Mic+Anl+LL	($F_{T,P}$=1)
vi:	Ne+Mic+Anl+Ab+LL	($F_{T,P}$=1)
vii:	Ne+Mic+Ab+Sod+LL	($F_{T,P}$=1)
viii:	Ne+Sod+Mic+Anl+Ab+LL	($F_{T,P}$=0)
*$F_{T,P}$: Number of free variables at constant T and P.		
**In sub-system SiO_2–Al_2O_3–SiO_2–H_2O–NaCl.		
LL: Lujavritic liquid.		
(c) Stability-constraining mineral-melt reactions		
Divariant reactions in log a_{NaCl}–log a_{SiO_2}–log a_{H_2O} space:		
A:	Ne+3[SiO_2]+[NaCl]=Sod+Mic	
B:	Ne+5 [SiO_2]+3 [H_2O]=3 Anl+Mi	
C:	Anl+[SiO_2]+[NaCl]=Sod+[H_2O]	
D:	Ne+8 [SiO_2]=3 Ab+Mic	
E:	3 Ne+6 Anl+5 [NaCl]=5 Sod+3 Mic+6 [H_2O]	

6.2. Early magmatic in situ layering

6.2.1. Microrhythmic layering in arfvedsonite lujavrite

Crystallization in the lujavrite magma was probably confined to a stagnant magma layer at the floor of the chamber. The crystallization front and resulting layers may have been on the centimetre scale, whereas the stagnant layer was many metres thick (cf. McBirney and Noyes, 1979).

The dark layers show primocrysts of nepheline, sodalite and microcline in a closely packed fine-grained matrix, and distinctly small amounts of interstitial analcime. This suggests that crystallization ended abruptly but there are no signs of a sudden loss of H_2O: no breaking of crystals or disturbance of lamination and no nearby veining. The light-coloured layers, in contrast, had a high proportion of H_2O-rich interstitial melt but there are no signs of its escape.

These features might suggest that each layer crystallized as a closed system from a well-defined liquid layer. Closed-system crystallization, however, does not provide a mechanism for producing a subsequent layer or sequence of layers of different chemistry. It seems more likely that each liquid layer was generated by open-system crystallization at the crystallization front. The microrhythmic character of the layering further requires that the stage of open crystallization started and finished abruptly and that subsequently there was little or no interaction between the layers.

The chemical compositions of the dark and light-coloured layers oscillate about the average composition of the arfvedsonite lujavrite in the Tunulliarfik area (Fig. 7). Oscillatory crystallization of cumulus phases around a cotectic has been reported from a number of layered basic/ultrabasic intrusions (i.e., Komor and Elthon, 1990; Volker and Upton, 1990). The layered lujavrites

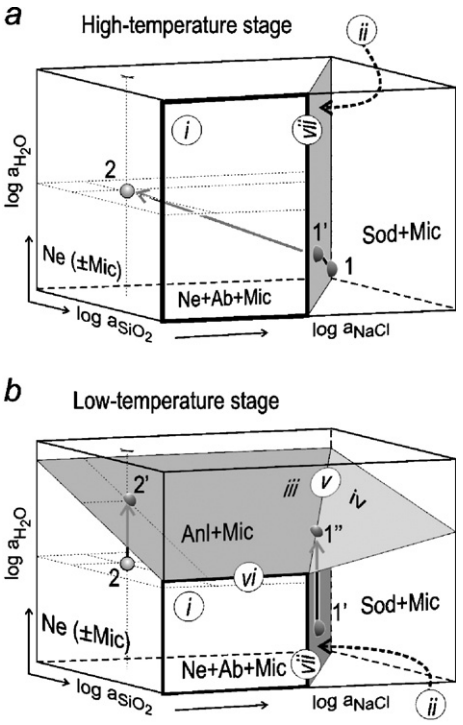

Fig. 10. Stability fields of liquidus mineral assemblages in lujavritic liquid in the Na_2O–Al_2O_3–SiO_2–K_2O–H_2O–NaCl system at constant pressure and temperature in log a_{NaCl}–log a_{SiO_2}–log a_{H_2O} space. The diagram shows the silica-undersaturated part of the activity space. The phase assemblage Ab+Ne+Mic+LL (i.e., a normal silica-buffered nepheline syenite mineral assemblage, LL=lujavritic liquid) is stable only within the part of the front face of the diagram outlined by a heavy contour; outside this area, albite is unstable as a liquidus mineral in lujavrite liquid. Numerals identify low-variance phase assemblages as given in Table 3b. See Sections 5 and 6.2.2 for further discussion. (a) High-temperature stage above the maximum stability field of liquidus analcime. Circles within the diagram illustrate the crystallization of a dark layer (1 to 1′), followed by the massive crystallization of nepheline in a light-coloured layer (towards point 2). (b) Low-temperature stage where analcime is stable at the liquidus. Crystallization of Ne will drive an interstitial liquid towards the stability field of Anl+Mic (at point 2′), where the remaining liquid is consumed. Dark layers follow a similar trend from 1′ to 1″. See Sections 5 and 6.2.2 for further discussion.

studied here were multiply saturated in nepheline, arfvedsonite, microcline, sodalite and eudialyte.

We consider that crystallization of a particular assemblage of cumulus and intercumulus phases in the dark layers, an assemblage with relatively high contents of sodalite, microcline and arfvedsonite, reduced the immediately adjacent liquid within the stagnant layer in the components of these phases (cf. McBirney and Noyes, 1979). This led the adjacent liquid to eventually crystallize a characteristic assemblage of minerals, in this case, an urtitic layer with distinctly high contents of nepheline, eudialyte and late-stage analcime. In addition, as the adjacent liquid layer developed, cations with high charges and/or large ionic radii, e.g., Al^{3+}, Zr^{4+}, would diffuse away more slowly (Hofmann, 1980) and this could also promote the crystallization of nepheline and eudialyte.

In general, the layers are characterized by significant amounts of early cumulus and intercumulus phases crystallizing over a short temperature interval (Piotrowski and Edgar, 1970) and by late interstitial minerals. This largely explains why the bulk chemistry of both layers has a liquid character, relatively close to the composition of the average arfvedsonite lujavrite (Fig. 7). The chemistry of both layers is best generalized as liquid-like but distorted by enhanced and reduced amounts of certain phases.

The character of the layers was closely linked to pronounced oscillations in the contents and activities of NaCl and H_2O adjacent to the crystallization front.

6.2.2. Rhythmic shifts in activities of volatiles

Repetitive changes between nepheline+sodalite +microcline-bearing dark layers and sodalite-free, microcline-poor urtitic layers reflect changes in the immediately parental melt compositions (liquid layers) and, hence, in the contents and activities of volatiles. They correspond to changes in component activities at high-*T* from plane ii (Ne+Sod+Mic+LL) into the primary liquidus field of Ne±Mic in Fig. 10a. The critical parameters for a shift across this plane are silica and NaCl activities (reaction A, Table 3c) and not water activity which is likely to rise as long as the total water content of the cumulate assemblages is less than the concentration of water in the magma.

Under the conditions of Fig. 10a, a dark layer starts when a liquid crystallizes Ne+Sod+Mic±Arf (point 1 in Fig. 10a). It could be argued that continued crystallization of Sod eventually exhausts the NaCl component, and the adjacent liquid layer shifts into the primary volume of Ne (towards point 2 in Fig. 10a) and begins crystallization of a nepheline-rich urtitic layer. This migration could take place immediately after crystallization of the sodalite-bearing primocrysts ceases since these primocrysts amount to ~30 vol.%. This is probably adequate to establish a high-viscosity layer (Marsh, 1996) able to provide a foundation for the urtitic layer to crystallize on. Continued extraction of K and Fe is required in order to establish the distinctive chemistry and mineralogy (microcline-, arfvedsonite-rich) of the dark layers.

During crystallization of the primocrysts, the residual liquid of the dark layer will evolve with increasing SiO_2 and H_2O along plane ii to point 1′ in Fig. 10a, without reaching the stability limit of albite. Simultaneously, increasing contents of K_2O and FeO_t will promote crystallization of Mic+Arf. These fine-grained intercumulus phases (~65 vol.%) probably crystallized rapidly and established a virtually solid character to the layer. Copious crystallization of Mic+Arf is also required to deplete components of these phases in the adjacent liquid layer (Section 6.2.1) and must have taken place during open-system crystallization. Note that component activities are confined to plane ii as long as Ne+Sod+Mic all crystallize together, i.e., throughout the dark layer. The limited experimental work on lujavrites (Section 5) allows us to propose that crystallization of primocrysts and intercumulus minerals was essentially a single high-*T* crystallization event, with the primocrysts growing to larger sizes. This would inhibit fractionation within the dark layers and lead to their isomodal character.

The preferred shift from point 1′ to 2 in Fig. 10a initiated crystallization within a light-coloured layer. During the high-*T* stage of open-system crystallization, abundant separation of nepheline and eudialyte rapidly established a highly viscous framework for the layer and the adjacent liquid layer acquired an increased a_{NaCl}. As a result, there would eventually be a shift back to the assemblage of Ne+Sod+Mic primocrysts in the next dark layer, and the cycle would start again.

The internal or in situ crystallization of dark and light-coloured layers is now considered. In dark layers, most in situ crystallization takes place at the high-*T* stage (Fig. 10a). Experimental work on lujavrites (Piotrowski and Edgar, 1970) points to a large temperature interval before significant in situ crystallization resumes at a low-*T*, high-a_{H_2O} interstitial stage (Fig. 10b, point 1″). The last few percent of melt crosses plane iii and crystallizes a small volume of interstitial Anl which replaces the margins of early Ne+Sod.

The light-coloured layers formed in two main crystallization stages. Abundant early crystallization of nepheline and eudialyte accompanied by minor

microcline, arfvedsonite and REE phosphate minerals generated an urtitic cumulate and an H_2O-rich intercumulus melt with higher a_{SiO_2} and especially higher a_{H_2O}. The intercumulus melt would migrate into the Anl±Mic field (point 2′ in Fig. 10b). There is clear evidence that the watery low-viscosity intercumulus melt was displaced upwards, i.e., fractionated within the urtitic layers. Crystallization of this melt was probably delayed to a low-*T* stage (Fig. 10b), at 500–400 °C, when abundant Anl crystallized and replaced much of the early Ne (reaction B in Table 3b), especially in the upper part of the layers. Arfvedsonite was replaced by aegirine, microcline by analcime, and a new low-*T* microcline crystallized (Section 3). The upper parts also show a decrease in Ca and Zr contents (eudialyte), but an increase in REE and P contents (REE phosphates) and in Zr/Hf and Nb/Ta ratios in eudialyte. Thus, in situ fractional crystallization led to increased a_{H_2O} and internal layering within the urtitic layers.

The crystallization history inferred for the urtitic layers implies that H_2O was largely retained in the layers. Given the long interval of consolidation of >250 °C in lujavrites (Section 5), the overlying dark layer must have largely solidified before the watery interstitial melts of the underlying urtitic layer consolidated. This is consistent with the local metasomatic formation, presumably by H_2O-rich residual fluids, of brown aegirine, analcime and new microcline in the lower margin of dark layers (Figs. 5 and 6).

6.3. Alternative origins for microrhythmic layering

6.3.1. Volatiles and pressure release

Clinopyroxene is the liquidus phase at $P_{H_2O}=1$ kbar, whereas eudialyte, nepheline and clinopyroxene are liquidus phases at $P_{H_2O}=0.5$ kbar in melting experiments on eudialyte lujavrite from Lovozero (Kogarko and Romanchev, 1983). This combined with the observation that decreasing P_{H_2O} is known to expand the nepheline field in silica-undersaturated melt systems (Gittins, 1979; Korobeinikov et al., 1998) suggests that, in the studied lujavrites, crystallization of light-coloured layers rich in nepheline and eudialyte was initiated by a pressure decrease and/or loss of volatiles.

Relief of pressure will generally be followed by a gradual recovery which should lead to a series of sharp-diffuse layer boundaries. The sharp lower contacts and the occasional diffuse upper contacts of the light-coloured layers are consistent with this prediction. Loss of volatiles, however, disagrees with the inference that the light-coloured layers formed from an H_2O-rich magma.

Changes in pressure and volatile contents could be a response to short-lived external events such as fracturing and collapse of the magma chamber roof or perhaps earthquakes. Igneous layering is more prominent in parts of layered intrusions where xenoliths or autoliths are abundant (McBirney and Noyes, 1979; Bird et al., 1985; Upton et al., 1996). At Tuttup Attakoorfia, however, density considerations and the continuity of features in adjacent naujaite rafts imply that the rafts are effectively in situ and result from a quiet process of piecemeal stoping (Sørensen et al., this volume). The rafts were more or less in position when the lujavritic magma developed its layering. In this context, it is worth recalling the statement of Brown (1956) that random external events can hardly produce regular layering.

6.3.2. A layered magma chamber

Plausible evidence has been presented for liquid layering of magma chambers at Ilímaussaq (Bailey, 1995; Bailey et al., 2001) and for crystallization of layered kakortokite from individual melt layers (Sørensen and Larsen, 1987). However, these are macro-scale phenomena which are thought to occur across the full width of the intrusion. In addition, it is difficult to envisage how a horizontally layered magma can produce the weakly undulating orientation of the microrhythmic lujavrite layers, and the locally vertical layers.

6.3.3. Late-stage in situ processes

Several late-stage processes have the potential to produce layered rocks. Examples include the interplay between compaction and rising intercumulus melts, the competitive growth of crystals, and the selective solution of earlier crystals followed by reprecipitation. Key criteria for these processes include Liesegang-type growth (McBirney and Noyes, 1979), broken and distorted crystals (Boudreau and McBirney, 1997), obliterated primary textures and associated pegmatites (Irvine et al., 1998), “doublet” layers (Boudreau, 1995), and lenticular or tapered layers (Cawthorn, 1994). All these features are absent in the layering studied here.

In fact, the late-stage minerals and textures in the layered lujavrites (see Section 3) have all been reported in earlier studies on non-layered Ilímaussaq lujavrites (Sørensen, 1962; Bailey and Gwozdz, 1994; Rose-Hansen and Sørensen, 2002; Sørensen et al., 2003) and do not call for special explanations. As argued above, many of the late magmatic processes in layers can be

traced back to characteristics that were established at an early stage.

6.4. Parental magma for microrhythmic layers

The bulk composition of the layered sequence compared to the background arfvedsonite lujavrites is characterized by high sodalite, Cl and S contents (Table 2). It is tempting to relate these features to reactions between arfvedsonite lujavrite and the enclosed sodalite-rich naujaite xenoliths. Naujaite has much higher contents of Al_2O_3 than the average arfvedsonite lujavrite (about 22% vs. 14.6%) and of Na_2O (about 15% vs. 10.7%) and only slightly higher contents of K_2O (about 4% vs. 3.3%). Therefore, bulk assimilation of naujaite will not yield the observed chemistry of the layered sequence. Sørensen (1962) showed that naujaite xenoliths in lujavrite are 'bleached' due to strong analcimization and our preliminary work demonstrates that bleached naujaite has increased levels of Na_2O and H_2O and low levels of K_2O. The bleaching may be related to exchange reactions between the naujaitic roof of the lujavritic magma chamber and the volatile-rich lujavritic magma. However, it is difficult to explain large-scale processes by diffusive exchange of material. The naujaite reaction mechanism, nevertheless, is an interesting possibility which deserves more detailed study.

7. Conclusions

(1) Microrhythmic layers, locally developed in agpaitic arfvedsonite lujavrites, are draped around naujaite rafts derived from the roof zone of the lujavrite magma chamber. The layers lack structures indicative of current processes or post-cumulus differentiation.

(2) Dark laminated isomodal layers enriched in early sodalite and intercumulus microcline and arfvedsonite alternate sharply with light-coloured granular urtitic layers. Dark layers are characterized by high contents of K–Cl–Fe (microcline, sodalite, arfvedsonite) and low contents of Na–H_2O–Zr–REE–P, whereas urtitic layers (nepheline, analcime, eudialyte, REE phosphates) show the opposite features. Urtitic layers display abundant early crystallization of nepheline; eudialyte concentrates at the base of a layer, whereas late-stage analcime and REE phosphates concentrate in the higher parts.

(3) The two types of layers have complementary chemical compositions and oscillate about the composition of the background arfvedsonite lujavrite.

(4) During crystallization of each layer at the crystallization front, components were selectively exchanged with the adjacent liquid layer. As the crystallization front advanced and crystallization began in this liquid layer, it started to exchange components with the overlying magma and thereby generated a new, complementary liquid layer. Oscillating activities of silica, H_2O and, antipathetically, NaCl are associated with an alternation of wet and dry layers enriched in analcime and sodalite, respectively.

(5) We speculate that the microrhythmic sequence developed from a K–Cl-rich but Na–H_2O-poor facies of arfvedsonite lujavrite which formed by exchanging components with the sodalite-rich naujaite rafts.

Acknowledgements

Field studies carried out by H.S. were supported by grants from the Danish Natural Science Research Council and the Carlsberg Foundation. The company of Henning Bohse, Mineral Development International A/S, in the field including boat transportation is especially acknowledged. L.N.K.'s visit to Copenhagen in autumn 2001 was funded by the Royal Danish Academy of Sciences and Letters. We thank Rajmund Gwozdz, Birgit Damgaard and the Rock Analysis Laboratory of the Denmark and Greenland Geological Survey for analytical data and Camilla Santaris, Britta Munch and Ole Bang Berthelsen for help in the preparation of the manuscript and illustrations. Constructive advice from the referees H.R. Naslund and A. E. Boudreau is gratefully acknowledged, and we thank Gregor Markl for much editorial encouragement along the way.

References

Andersen, T., Sørensen, H., 2005. Stability of naujakasite in hyperagpaitic melts, and the petrology of naujakasite lujavrite in the Ilímaussaq alkaline complex, South Greenland. Mineralogical Magazine 69, 125–136.

Andersen, S., Bohse, H., Steenfelt, A., 1981. A geological section through the southern part of the Ilímaussaq intrusion. Rapport-Grønlands Geologiske Undersøgelse 103, 39–42.

Bailey, J.C., 1995. Cryptorhythmic and macrorhythmic layering in aegirine lujavrite, Ilímaussaq alkaline intrusion, South Greenland. Bulletin of the Geological Society of Denmark 42, 1–16.

Bailey, J.C., Gwozdz, R., 1994. Li distribution in aegirine lujavrite, Ilímausssaq alkaline intrusion, South Greenland: role of cumulus and post-cumulus processes. Lithos 31, 207–225.

Bailey, D.K., Schairer, J.F., 1966. The system Na_2O–Al_2O_3–Fe_2O_3–SiO_2 at 1 atmosphere, and the petrogenesis of alkaline rocks. Journal of Petrology 7, 114–170.

Bailey, J.C., Gwozdz, R., Rose-Hansen, J., Sørensen, H., 2001. Geochemical overview of the Ilímaussaq alkaline complex, South Greenland. Geology of Greenland Survey Bulletin 190, 35–54.

Bird, D.K., Rosing, M.T., Manning, C.E., Rose, N.M., 1985. Geologic field studies in the Miki Fjord area, East Greenland. Bulletin of the Geological Society of Denmark 34, 219–236.

Bohse, H., Andersen, S., 1981. Review of the stratigraphic divisions of the kakortokite and lujavrite in southern Ilímaussaq. Rapport-Grønlands Geologiske Undersøgelse 103, 53–62.

Boudreau, A.E., 1995. Crystal aging and the formation of fine-scale igneous layering. Mineralogy and Petrology 54, 55–69.

Boudreau, A.E., McBirney, A.R., 1997. The Skaergaard Layered Series: Part III. Non-dynamic layering. Journal of Petrology 38, 1003–1020.

Brown, G.M., 1956. The layered ultrabasic rocks at Rhum, Inner Hebrides. Philosophical Transactions of the Royal Society of London. B 240 (53 pp.).

Carmichael, I.S.E., Turner, F.J., Verhoogen, J., 1974. Igneous Petrology. McGraw-Hill, New York. 739 pp.

Cawthorn, R.G., 1994. Growth nodes at the base of magnetite layers in the upper zone of the Bushveld Complex. South African Journal of Geology 97, 455–461.

Edgar, A.D., 1974. Experimental studies. In: Sørensen, H. (Ed.), The Alkaline Rocks. John Wiley & Sons, London, pp. 355–389.

Edgar, A.D., Nolan, J., 1966. Phase relations in the system $NaAlSi_3O_8$ (albite)–$NaAlSiO_4$ (nepheline)–$NaFeSi_2O_6$ (acmite)–$CaMgSi_2O_6$ (diopside)–H_2O and its importance in the genesis of alkaline undersaturated rocks. Mineralogical Society of India, IMA Volume 1966, pp. 175–181.

Ferguson, J., 1964. Geology of the Ilímaussaq alkaline intrusion, South Greenland. Bulletin Grønlands Geologiske Undersøgelse 39, 82 pp. (also Meddelelser om Grønland 172(4)).

Gerasimovsky, V.I., 1969. Geochemistry of the Ilímaussaq Alkaline Complex. Nauka, Moscow. 174 pp. (in Russian).

Gittins, J., 1979. The feldspathoidal alkaline rocks. In: Yoder Jr., H. S. (Ed.), The Evolution of the Igneous Rocks. Fiftieth Anniversary Perspectives. Princeton University Press, Princeton, NJ, pp. 351–390.

Hofmann, A.W., 1980. Diffusion in natural silicate melts. In: Hargraves, R.B. (Ed.), Physics of Magmatic Processes. Princeton University Press, Princeton, pp. 385–417.

Irvine, T.N., 1987. Glossary of terms for layered intrusions. In: Parsons, I. (Ed.), Origins of Igneous Layering. D. Reidel, Dordrecht, pp. 641–647.

Irvine, T.N., Andersen, J.C.O., Brooks, C.K., 1998. Included blocks (and blocks within blocks) in the Skaergaard intrusion: geologic relations and the origins of rhythmically modally graded layers. Bulletin of the Geological Society of America 119, 1398–1447.

Kogarko, L.N., Romanchev, B.P., 1983. Phase equilibria in alkaline melts. International Geology Review 25, 534–546 (Translated from Zapiski Vsesoyuznogo Mineralogicheskogo Obshchestva 1982, 2, 167–182 (in Russian)).

Komor, S.C., Elthon, D., 1990. Formation of anorthosite–gabbro rhythmic phase layering: an example at North Arm Mountain, Bay of Islands ophiolite. Journal of Petrology 31, 1–50.

Konnerup-Madsen, J., Rose-Hansen, J., 1984. Composition and significance of fluid inclusions in the Ilímaussaq peralkaline granite, South Greenland. Bulletin de Minéralogie 107, 317–326.

Korobeinikov, A., Dubrovskii, M., Laajoki, K., Gehör, S., 1998. Phase equilibria in the undersaturated part of Petrogeny's residua system: a preliminary graphical analysis of its potassic field with potential implications for the origin of pseudoleucite. Neues Jahrbuch für Mineralogie Monatshefte 1998 (6), 241–252.

Kystol, J., Larsen, L.M., 1999. Analytical procedures in the Rock Geochemical Laboratory of the Geological Survey of Denmark and Greenland. Geology of Greenland Survey Bulletin 184, 59–62.

Larsen, L.M., Sørensen, H., 1987. The Ilímaussaq intrusion—progressive crystallization and formation of layering in an agpaitic magma. In: Fitton, J.G., Upton, B.G.J. (Eds.), Alkaline Igneous Rocks. Special Publication Geological Society (London), vol. 30, pp. 473–488.

Maaløe, S., 1978. The origin of rhythmic layering. Mineralogical Magazine 42, 337–345.

Markl, G., Marks, M., Schwinn, G., Sommer, H., 2001. Phase equilibrium constraints on intensive crystallization parameters of the Ilímaussaq complex, South Greenland. Journal of Petrology 42, 2231–2258.

Marsh, B.D., 1996. Solidification fronts and magmatic evolution. Mineralogical Magazine 60 (398), 5–40.

McBirney, A.R., Noyes, R.M., 1979. Crystallization and layering of the Skaergaard intrusion. Journal of Petrology 20, 487–554.

McDonough, W.F., Sun, S.-S., 1995. The composition of the Earth. Chemical Geology 120, 223–253.

Naslund, H.R., McBirney, A.R., 1996. Mechanisms of formation of igneous layering. In: Cawthorn, R.G. (Ed.), Layered Igneous Rocks. Elsevier, Amsterdam, pp. 1–44.

Nolan, J., 1966. Melting-relations in the system $NaAlSi_3O_8$–$NaAlSiO_4$–$NaFeSi_2O_6$–$CaMgSi_2O_6$–H_2O and their bearing on the genesis of alkaline undersaturated rocks. Quarterly Journal of the Geological Society of London 122, 119–157.

Norrish, K., Chappel, B.W., 1977. X-ray fluorescence spectrometry, In: Zussman, J. (Ed.), Physical Methods in Determinative Mineralogy, 2nd ed. Academic Press, London, pp. 201–272.

Piotrowski, J.M., Edgar, A.D., 1970. Melting relations of undersaturated alkaline rocks from South Greenland compared to those of Africa and Canada. Meddelelser om Grønland 181 (9) (62 pp.).

Rose-Hansen, J., Sørensen, H., 2002. Geology of lujavrites from the Ilímaussaq alkaline complex, South Greenland with information from seven bore holes. Greenland Geoscience 40 (58 pp.).

Semenov, E.I., 1969. Mineralogy of the Ilímaussaq Alkaline Massif. Nauka, Moscow. 165 pp. (in Russian).

Sørensen, H., 1962. On the occurrence of steenstrupine in the Ilímaussaq massif, southwest Greenland. Bulletin Grønlands Geologiske Undersøgelse 32. 251 pp. (also Meddelelser om Grønland 167(1)).

Sørensen, H., 2001. Brief introduction to the geology of the Ilímaussaq alkaline complex, South Greenland, and its exploration history. Geology of Greenland Survey Bulletin 190, 7–24.

Sørensen, H., Larsen, L.M., 1987. Layering in the Ilímaussaq alkaline intrusion, South Greenland. In: Parsons, I. (Ed.), Origins of Igneous Layering. D. Reidel, Dordrecht, pp. 1–28.

Sørensen, H., Bailey, J.C., Kogarko, L.N., Rose-Hansen, J., Karup-Møller, S., 2003. Spheroidal structures in arfvedsonite lujavrite, Ilímaussaq alkaline complex, South Greenland—an example of macro-scale liquid immiscibility. Lithos 70, 1–20.

Sørensen, H., Bohse, H., Bailey, J.C., this volume. The origin and mode of emplacement of lujavrites in the Ilímaussaq alkaline complex, South Greenland.

Tuttle, O.F., Bowen, N.L., 1958. Origin of granite in the light of experimental studies in the system $NaAlSi_3O_8$–$KAlSi_3O_8$–SiO_2–H_2O. Memoir-Geological Society of America 74 (153 pp.).

Upton, B.G.J., Parsons, I., Emeleus, C.H., Hodson, M.E., 1996. Layered alkaline igneous rocks of the Gardar Province, South Greenland. In: Cawthorn, R.G. (Ed.), Layered Intrusions. Elsevier, Amsterdam, pp. 331–363.

Ussing, N.V., 1912. Geology of the country around Julianehaab, Greenland. Meddelelser om Grønland 38 (426 pp.).

Volker, J.A., Upton, B.G.J., 1990. The structure and petrogenesis of the Trallval and Ruinsival areas of the Rhum ultrabasic complex. Transactions of the Royal Society of Edinburgh. Earth Sciences 81, 69–88.

Wager, L.R., 1959. Differing powers of crystal nucleation as a factor producing diversity in layered igneous intrusions. Geological Magazine 96, 75–80.

Wager, L.R., Brown, G.M., 1968. Layered Igneous Rocks. Oliver and Boyd, Edinburgh. 538 pp.